


## ORIGINAL ARTICLE

# Early-Emerging Sulcal Patterns Are Atypical in Fetuses with Congenital Heart Disease

Cynthia M. Ortinau<sup>1,2</sup>, Caitlin K. Rollins<sup>3,4</sup>, Ali Gholipour<sup>5,6</sup>, Hyuk Jin Yun <sup>7,8,9</sup>, Mackenzie Marshall<sup>7</sup>, Borjan Gagoski<sup>5,6,7</sup>, Onur Afacan<sup>5,6</sup>, Kevin Friedman<sup>8,10</sup>, Wayne Tworetzky<sup>8,10</sup>, Simon K. Warfield<sup>5,6</sup>, Jane W. Newburger<sup>8,10</sup>, Terrie E. Inder<sup>2,8</sup>, P. Ellen Grant<sup>5,6,7,9</sup> and Kiho Im<sup>7,8,9</sup>

<sup>1</sup>Department of Pediatrics, Washington University in St. Louis, St. Louis, MO 63110, USA, <sup>2</sup>Department of Pediatric Newborn Medicine, Brigham and Women's Hospital, Boston, MA 02115, USA, <sup>3</sup>Department of Neurology, Boston Children's Hospital, Boston, MA 02115, USA, <sup>4</sup>Department of Neurology, Harvard Medical School, Boston, MA 02115, USA, <sup>5</sup>Department of Radiology, Boston Children's Hospital, Boston, MA 02115, USA, <sup>6</sup>Department of Radiology, Harvard Medical School, Boston, MA 02115, USA, <sup>7</sup>Fetal Neonatal Neuroimaging and Developmental Science Center, Boston Children's Hospital, Boston, MA 02115, USA, <sup>8</sup>Department of Pediatrics, Harvard Medical School, Boston, MA 02115, USA, <sup>9</sup>Division of Newborn Medicine, Boston Children's Hospital Boston, MA 02115, USA and <sup>10</sup>Department of Cardiology, Boston Children's Hospital Boston, MA 02115, USA

Address correspondence to Cynthia M. Ortinau, Washington University in St. Louis, 660 South Euclid, Campus Box 8116, St. Louis, MO 63110, USA. Email: ortinau\_c@wustl.edu; Kiho Im, Boston Children's Hospital, 401 Park Drive, Boston, MA 02115, USA. Email: kiho.im@childrens.harvard.edu

Cynthia M. Ortinau and Caitlin K. Rollins contributed equally to this work.

## Abstract

Fetuses with congenital heart disease (CHD) have third trimester alterations in cortical development on brain magnetic resonance imaging (MRI). However, the intersulcal relationships contributing to global sulcal pattern remain unknown. This study applied a novel method for examining the geometric and topological relationships between sulci to fetal brain MRIs from 21–30 gestational weeks in CHD fetuses ( $n = 19$ ) and typically developing (TD) fetuses ( $n = 17$ ). Sulcal pattern similarity index (SI) to template fetal brain MRIs was determined for the position, area, and depth for corresponding sulcal basins and intersulcal relationships for each subject. CHD fetuses demonstrated altered global sulcal patterns in the left hemisphere compared with TD fetuses (TD [SI, mean  $\pm$  SD]:  $0.822 \pm 0.023$ , CHD:  $0.795 \pm 0.030$ ,  $P = 0.002$ ). These differences were present in the earliest emerging sulci and were driven by differences in the position of corresponding sulcal basins (TD:  $0.897 \pm 0.024$ , CHD:  $0.878 \pm 0.019$ ,  $P = 0.006$ ) and intersulcal relationships (TD:  $0.876 \pm 0.031$ , CHD:  $0.857 \pm 0.018$ ,  $P = 0.033$ ). No differences in cortical gyrification index, mean curvature, or surface area were present. These data suggest our methods may be more sensitive than traditional measures for evaluating cortical developmental alterations early in gestation.

**Key words:** brain, congenital heart disease, fetus, magnetic resonance imaging, sulcal pattern

Congenital heart disease (CHD) is a structural defect of the heart that can result in substantial morbidity and the need for lifelong medical care. Neurodevelopmental impairment is increasingly recognized as the most common morbidity in this population and occurs in up to 50% of children with moderate to severe CHD (Wernovsky 2006; Miatton et al. 2007; Majnemer et al. 2008; Bellinger et al. 2011; Goldberg et al. 2014). Despite the high frequency of neurodevelopmental sequelae, the underlying neural mechanisms that place children with CHD at risk are not fully understood. Postnatal brain magnetic resonance imaging (MRI) studies have offered some insight by identifying high rates of brain injury and aberrations in brain development. Of particular interest is the presence of altered brain development even before cardiac surgery, which suggests an in utero vulnerability (Mahle et al. 2002; Miller et al. 2007; Licht et al. 2009; Ortinau et al. 2012, 2013; Beca et al. 2013; Algra et al. 2014). Recent fetal MRI studies in CHD have supported this hypothesis by demonstrating smaller brain volume, decreased cortical surface area, impaired gyrification, and altered sulcation during the third trimester of pregnancy, a period of rapid brain development and vulnerability, especially with regard to cortical development (Limperopoulos et al. 2010; Clouchoux et al. 2013; Sun et al. 2015; Masoller et al. 2016). Disturbances in cell proliferation, differentiation, migration, and organization can each lead to abnormalities in cortical development (Fogliarini et al. 2005). Thus, characterization of the exact timing and pattern of cortical disturbances in the CHD population could help to distinguish underlying mechanisms of altered development (e.g., genetically driven changes vs. cerebral hemodynamic alterations from the cardiac defect).

Quantitative MRI methods have been used to evaluate the morphological development of the cerebral cortex. These methods include curvature-based measures such as mean curvature, the gyrification index (GI), and sulcal analysis using area, depth, and length. Existing CHD studies, including our own, have used such methods to define cortical development in this population (Awate et al. 2009; Clouchoux et al. 2013; Ortinau et al. 2013). However, these methods do not provide a means to characterize the interrelated arrangement and global patterning of sulci using the relationship between sulci. The intersulcal relationship and global sulcal pattern are thought to be an important part of the ultimate structural anatomy of the cortex and the organization of cortical functional areas and white matter connections (Van Essen 1997; Klyachko and Stevens 2003; Fischl et al. 2008; Sun and Hevner 2014). In addition, our previous studies have shown these relationships and patterns to reflect genetically influenced cortical development (Im, Pienaar, Lee et al. 2011; Im, Pienaar, et al. 2013; Im et al. 2016). Therefore, application of a technique that allows assessment of intersulcal relationships may provide additional insight into altered brain development in CHD.

Our group has developed a method for determining the spatial, geometric, and topological relationships between sulci to more completely characterize sulcal patterns (Im, Pienaar, Lee et al. 2011). Application of this technique has supported a genetic impact on the sulcal pattern from twin pairs (Im, Pienaar, Lee et al. 2011) and has shown atypical cortical development in children with polymicrogyria and developmental dyslexia (Im, Pienaar, et al. 2013; Im et al. 2016). Recently, an atypical early sulcal pattern was revealed in human fetuses with brain abnormalities and agenesis of the corpus callosum using this method, while GI showed no difference, suggesting sulcal pattern analysis may be more sensitive for early cortical disturbances (Im et al. 2017; Tarui et al. 2018). Here, we sought

to apply this technique to evaluate for early differences in sulcal patterns between CHD and typically developing (TD) fetuses. We hypothesized that fetuses with CHD would have altered sulcation patterns in the early third trimester of pregnancy.

## Materials and Methods

### Study Subjects

This cohort is a part of an ongoing prospective longitudinal study investigating brain development in CHD fetuses compared with TD fetuses cared for in the Advanced Fetal Care Center at Boston Children's Hospital. Inclusion criteria for the CHD group were pregnant women aged 18–45 years with a fetal diagnosis of moderate to severe CHD and a gestational age of 18–30 weeks. Moderate to severe CHD was defined as any cyanotic heart disease, atrioventricular septal defect, large ventricular septal defect, moderate or severe aortic stenosis, moderate or severe pulmonary stenosis, and coarctation of the aorta (Hoffman and Kaplan 2002). Control subjects were pregnant women with a family history of CHD who were evaluated in the Advanced Fetal Care Center at Boston Children's Hospital but who had a normal fetal echocardiogram. Exclusion criteria for CHD and TD fetuses included maternal CHD, multiple gestation pregnancy, known congenital infection, fetal dysmorphic features on ultrasound, fetal brain malformations or other brain lesions, known fetal chromosomal abnormalities, or other identified fetal non-neurological anomalies. Mothers of CHD and TD fetuses were excluded after enrollment if the research MRI identified a previously unknown congenital anomaly that involved the brain or had known associations with abnormal neurodevelopment. Subjects with isolated mild ventriculomegaly were not excluded if they were a CHD fetus, as this finding has been reported in CHD but is of unknown clinical significance (Brossard-Racine et al. 2016). The study was approved by the local Institutional Review Board at Boston Children's Hospital and Brigham and Women's Hospital and written informed consent was obtained from all participants.

### MRI Acquisition, Processing, and Identification and Measurement of Sulcal Basins

Fetal brain MRI was performed without maternal sedation on a 3-Tesla MAGNETOM Skyra (Siemens Healthcare) equipped with an 18-channel body matrix coil. A T<sub>2</sub>-weighted Half-Fourier Acquisition Single-Shot Turbo Spin-Echo (HASTE) sequence was repeatedly performed in different orthogonal planes, with four to five acquisitions in each plane, as previously described (Gholipour et al. 2017). Data were acquired with an echo time of 100 and 120 ms, repetition time of 1.4–2.0 s, variable field of view dependent on fetal and maternal size, 256 × 204, 256 × 256, or 320 × 320 acquisition matrices (in-plane resolution of 1 mm), and slice thickness of 2–4 mm depending on fetal size, fetal motion, and signal to noise.

Multiple acquisition sets were used to generate an isotropic high-resolution volume reconstruction at 0.75 mm (Gholipour et al. 2010; Kuklisova-Murgasova et al. 2012), which was then manually aligned along the anterior and posterior commissure using AFNI ([afni.nimh.nih.gov/afni](http://afni.nimh.nih.gov/afni)) (Cox 2012). A semi-automated segmentation of the cortical plate was generated using an intensity value range and then manually refined by examining the segmentation on orthogonal planes in FreeView ([surfer.nmr.mgh.harvard.edu](http://surfer.nmr.mgh.harvard.edu)). The inner volume of the cortical plate was binarized and smoothed using a 3 × 3 × 3 voxel mean filter

for the reconstruction of smooth surface models that are less susceptible to noise. The 3D inner cortical plate surface was reconstructed using the isosurface function with an isovalue of 0.5 (Im et al. 2017; Tarui et al. 2018). Although small folds of similar size to a voxel might be eliminated, smoothing effectively limits noise and voxelized representation of the brain surface.

FreeSurfer software (surfer.nmr.mgh.harvard.edu) (Fischl 2012) was used to generate the mean curvature and depth maps from the 3D inner cortical plate surface reconstruction. For sulcal pattern analysis, sulcal catchment basins, defined as substructures decomposed from one large part of sulcal folds by convex ridges, were identified from the cortical surface. The sulcal basins were used as a basic element for sulcal pattern analysis because their spatial distribution is relatively invariant between subjects and hypothesized to relate to functional areas and activations (Derrfuss et al. 2009; Im et al. 2010). Sulcal basins were extracted onto cortical surface meshes with a watershed segmentation algorithm from the curvature map. In order to prevent overextraction of the segments in the watershed process, the curvature map was smoothed using a surface-based heat kernel with a full-width half-maximum value of 5 mm (Chung et al. 2005), and our watershed process merged small and shallow folds to remove noisy sulcal basins. Then a mean 3D relative position from 0 to 1 ( $x$ : left–right [0–1];  $y$ : posterior–anterior [0–1];  $z$ : inferior–superior [0–1]) was measured for each sulcal basin. The normalized surface area (area/whole cortical area) and mean depth of the sulcal basin were also calculated for sulcal geometry (Im et al. 2017; Tarui et al. 2018).

The sulcal pattern analysis methods employed here have been shown to have high reproducibility and reliability in adults across different scan sessions (up to 3 weeks apart) and different MR scanners, with a similarity of more than 0.90 for most cases. This study also demonstrated similarity of more than 0.85 across two MRI pipelines (the Montreal Neurological Institute and FreeSurfer), including tissue segmentation and

surface extraction (Im, Lee, et al. 2013). To demonstrate similar reliability of these methods in the fetal population, cortical plate segmentations were generated by two independent raters on two TD subjects from this cohort. The cortical plate surfaces were then extracted and sulcal basins were identified as outlined in the above methods for each of these segmentations. Supplementary Figure 1 visually demonstrates the high similarity of the number and spatial pattern of sulcal basins across these two raters.

## MRI Processing and Anatomical Sulcal Labeling for Fetal Brain Templates

Previously published fetal template brains (brain-development.org/brain-atlases) (Serag et al. 2012) ranging from 23 to 31 gestational weeks (GWs) were used as a reference for comparison of individual fetal brains. The cortical plate surface reconstruction and the identification and geometric measurements of sulcal basins were calculated for the fetal templates as described above (Im et al. 2017; Tarui et al. 2018).

To perform regional analysis based on a developmental timeline of sulcal folding, we manually assigned 19 anatomical labels of primary sulci to the sulcal basins of the nine templates (Sylvian fissure [SF], central sulcus [CS], superior frontal sulcus [SFS], middle frontal sulcus [MFS], inferior frontal sulcus [IFS], precentral sulcus [PrCS], postcentral sulcus [PoCS], intraparietal sulcus [IPS], subparietal sulcus [SPS], superior temporal sulcus [STS], inferior temporal sulcus [ITS], occipitotemporal sulcus [OTS], collateral sulcus [CoS], orbital sulcus [OrS], olfactory sulcus [OIS], cingulate sulcus [CiS], lateral occipital sulcus [LOS], calcarine sulcus [CaS], and parieto-occipital sulcus [POS]) (Fig. 1).

The gross temporal pattern of sulcal emergence was defined by assessing the formation of sulci on the cortical surfaces of the fetal templates and reviewing sulcation timetables that were previously reported based on neuropathology and MRI. Although absolute time points of the emergence for each

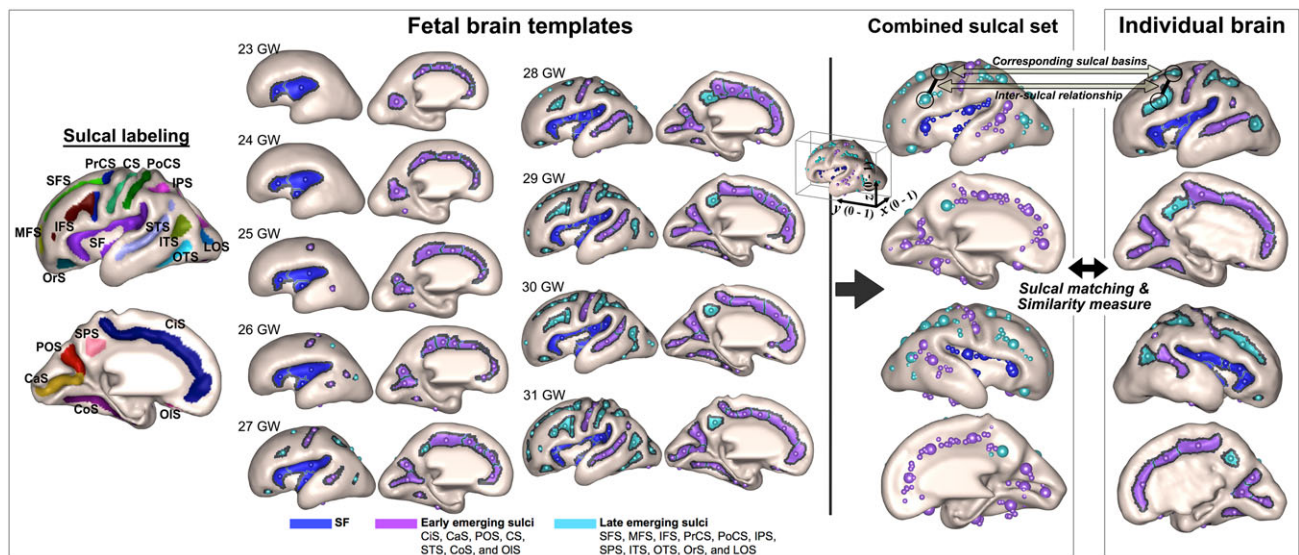


**Figure 1.** Manually assigned anatomical labels are demonstrated in the sulcal labeling figure and included the SF, CS, SFS, MFS, IFS, PrCS, PoCS, IPS, SPS, STS, ITS, OTS, CoS, OrS, OIS, CiS, LOS, CaS, and POS. The SF (blue), early-emerging sulci (purple), and late-emerging sulci (aqua) are highlighted on the fetal brain templates with each sulcal basin represented by a circle. The combined sulcal set represents the sulcal basin features of the corresponding sulcal basins as well as the features of the intersulcal relationship, which were generated for the fetal brain templates and each individual brain for sulcal matching and comparison of the similarity measures of individuals with the template.



sulcus demonstrated variability across these studies, the gross sulcal developmental timeline was consistent. Development of the SF occurs early in gestation, before 20 GWs, via a different mechanism than that of other cortical sulci. The SF develops after the initial telencephalic flexure and mainly results from external mechanical forces, whereas cortical sulci and gyri result predominantly from internal forces. After 20 GWs, operculization starts and the insular cortex is finally engulfed by the enlarged parietal, temporal, and frontal opercula (Afif et al. 2007; Sarnat and Flores-Sarnat 2016). The CiS, CaS, and POS are typically visible in the mid-second trimester of pregnancy, before 20 GW, and were categorized as the first-emerging sulci. The CS, STS, CoS, and OLS were visible later in the second trimester, typically 20–23 GW, and were categorized as the second-emerging sulci and all other sulci were regarded as the late-emerging sulci as they were not present until the third trimester (Fig. 1) (Chi et al. 1977; Garel et al. 2001; White et al. 2010; Habas et al. 2012; Clouchoux et al. 2013). This temporal information of developing sulcal folding was utilized for automatic regional analysis in individual fetal brains to investigate group differences in sulcal pattern of the SF (examined separately because it has an alternate developmental origin), early (first plus second)-emerging sulci, and late-emerging sulci. The global sulcal pattern analysis combined the results from the SF and early- and late-emerging sulci. The SF was included in this global analysis because the sulcal basins and pattern in the insular region reflect the gyral expansion and folding near the perisylvian region, where there may also be a contribution of internal forces for formation. Also, operculization of the SF is one of the main landmarks of the gyrification process and has been shown to be abnormal in fetuses with several cortical malformations (Guibaud et al. 2008; Lerman-Sagie and Malinger 2008; Sarnat and Flores-Sarnat 2016).

### Quantitative Sulcal Pattern Analysis

A detailed explanation of the methods has been previously reported (Im, Pienaar, Lee et al. 2011; Im, Pienaar, et al. 2013; Im et al. 2017), and we summarize herein. Each individual fetal brain was quantitatively compared with the combined set of nine template fetal brains and a similarity index (SI) was measured. Because temporal patterns of sulcal folding are variable across individuals and the CHD fetuses may show delayed sulcal development or more variable sulcal patterns, we employed the sulcal set of all template brains ranging from 23–31 GWs in an unbiased manner for sulcal pattern matching and the similarity measure rather than using a specific template of similar ages and assuming the optimal match was of the same GW. Sulcal pattern was represented by a feature set of sulcal basins (3D position, area, and depth of the sulcal basin) and included not only the local sulcal features but also the intersulcal geometric relationships in the left and right hemispheres. Each sulcal basin of an individual brain was optimally matched with one of the sulcal basins of the template brains, and their correspondence was defined using a spectral matching technique (Leordeanu and Hebert 2005). Through this matching process, sulcal basins of an individual brain were labeled based on the pre-labeled sulci on the template brains (Fig. 1).

Geometric similarities between corresponding sulcal basins were measured using 3D position, area, and depth of the sulcal basin to compare the sulcal set to that of the nine fetal brain templates. In addition, intersulcal geometric relationships (intersulcal differences of 3D position, area, and depth

relationships) were used to determine the intersulcal arrangement and patterning and were compared between individual and template brains. Sulcal pattern similarity to the templates, the SI, was defined as the mean of the similarities of all corresponding sulcal basins and the intersulcal relationships, which ranged from 0 to 1. Measures closer to one indicate increasing similarity to the template atlas. SI was measured globally for the whole brain, including all sulci. Moreover, we separately measured the similarities from the comparison of corresponding sulcal basins ( $SI_a$ ) and the comparison of intersulcal relationships ( $SI_b$ ), respectively, between individual and template brains. In particular, the  $SI_b$  is biologically and methodologically meaningful as it compares the intrinsic sulcal pattern that is minimally influenced by overall brain size, shape, and orientation, overall spatial shift of sulcal folding, and other confounding factors (Im, Pienaar, Lee et al. 2011; Tarui et al. 2018). In our recent study of fetuses with agenesis of corpus callosum, the major feature driving altered sulcal patterns in these fetuses was the intersulcal geometric relationships (Tarui et al. 2018).

In addition to the global measures, which included all fissures and visible sulci, subsets of all sulcal basins were examined in relation to the sulcal developmental timeline outlined above to test if atypical folding patterns were present in relation to a developmental trajectory that would suggest second trimester alterations. To do so, we measured the SI for the set of early-emerging sulci alone and then the set of late-emerging sulci. We also investigated the SF separately since this region has an alternate developmental origin than cortical sulci, as discussed above (Afif et al. 2007; Sarnat and Flores-Sarnat 2016). This method also allowed us to further calculate SI only using each individual feature by setting all weights of the other features to zero to assess their relative importance on sulcal pattern similarity.

### Cortical Surface Area, Mean Curvature, and GI

Cortical plate surface area, mean curvature, and 3D GI of the whole brain were calculated in order to evaluate for group differences with previously reported, “traditional” surface-based measures. The GI is defined as the ratio of the whole cortical surface to their outer, convex hull surface area (Zilles et al. 1988). A 3D morphological closing operation was performed for the inner volume of the cortical plate surface using a sphere of 15 mm diameter to close the sulcal folding (Schaer et al. 2008; Im et al. 2017). The outer hull surface wrapping the cortical plate surface was created from the binary closed volume using the isosurface function, and the 3D global GI of the entire left and right cerebral hemispheres was calculated.

### Statistical Analysis

Group comparisons of demographic and clinical characteristics were undertaken using an independent sample t-test or Fisher’s exact test when appropriate. The SI for the entire sulcal pattern of the left and right hemispheres was compared between the two groups for the combined set of all three features (3D position, sulcal area, and sulcal depth of the sulcal basin), as well as each individual feature, using an independent sample t-test. Similar analyses were performed for  $SI_a$  and  $SI_b$ . A false discovery rate (FDR) control was used at a  $q$  value of 0.05 to correct for multiple comparisons (Benjamini and Hochberg 1995; Genovese et al. 2002). Because of the possibility of sex-specific variations in sulcal patterns, group

comparisons were also undertaken separately for male and female fetuses. Subanalyses were performed for significant sulcal pattern measures from the global analysis to evaluate differences in the SF and in early- and late-emerging sulci by comparing the SI of the combined and individual features that demonstrated significance in the primary analysis. Sulcal pattern analyses were performed using “similarity” to the templates and sulcal pattern similarities were not theoretically or empirically associated with GWs (Im et al. 2017; Tarui et al. 2018). However, because of the wide range and slightly variable distribution of GWs in the cohort, linear regression was performed for all analyses to adjust for gestational age at MRI, where the measure was the dependent variable, the group was the independent variable, and gestational age at MRI was the covariate.

Finally, group comparisons were also undertaken for traditional surface-based measures, including GI, mean curvature, and surface area. Each of these measures changes significantly during fetal development and, again, there was a wide range in the GWs of the fetuses, therefore linear regression was also performed for these comparisons to adjust for gestational age at MRI.

## Results

### Patient Population

Seventeen TD fetuses and 19 CHD fetuses were included in the analysis (Table 1). There were no differences in maternal ethnicity ( $P = 0.605$ ), fetal sex ( $P = 1.000$ ), or gestational age at fetal MRI ( $P = 0.374$ ) between the two groups. Fetal MRI was performed at a mean  $\pm$  standard deviation (SD) of  $26.3 \pm 1.6$  GWs for the TD fetuses compared with  $26.9 \pm 2.5$  GWs for the CHD fetuses, with a range of 21.1–30.1 GWs for the entire cohort. None of the CHD fetuses had known syndromic/genetic diagnoses at the time of recruitment and there were no known new genetic diagnoses made after birth. One CHD fetus had mild unilateral ventriculomegaly (measuring 12 mm) detected on fetal MRI without any other structural abnormalities. A second CHD fetus (with hypoplastic left heart syndrome and intact atrial septum) had dilated pulmonary lymphatics noted on MRI, consistent with the underlying cardiac diagnosis. All other CHD fetuses had qualitatively normal MRIs. Three of the TD fetuses had incidental findings. One TD fetus had an isolated periventricular cyst. Two TD fetuses had mild ventricular asymmetry, but both lateral ventricles measured within the

**Table 1** Clinical characteristics of enrolled subjects

	GW at MRI	Fetal sex	Diagnosis
Subject 1	24.29	Male	d-TGA with intact ventricular septum
Subject 2	24.29	Male	Coarctation of the aorta with small left-sided structures and retrograde aortic arch flow
Subject 3	21.14	Male	TOF with absent pulmonary valve and moderate right ventricular dysfunction and dilation
Subject 4	29.43	Male	DORV with d-TGA, subpulmonary VSD, and hypoplastic aortic arch
Subject 5	30.14	Male	d-TGA with intact ventricular septum
Subject 6	28.43	Male	DORV with d-TGA and hypoplastic aortic valve and aortic arch
Subject 7	26.14	Female	Fetal aortic stenosis with evolving HLHS, status post fetal aortic valvuloplasty
Subject 8	29.14	Male	Unbalanced, right dominant, common AVC with DORV
Subject 9	27.14	Male	Fetal aortic stenosis with mild to moderate mitral regurgitation and retrograde aortic arch flow
Subject 10	24.86	Female	Unbalanced, right dominant, common AVC with likely coarctation of the aorta
Subject 11	22.57	Female	TOF with moderately hypoplastic pulmonary valve
Subject 12	29.43	Female	TOF with pulmonary atresia and major aortopulmonary collateral arteries
Subject 13	27.29	Male	DORV with d-TGA, mitral atresia, and hypoplastic left ventricle
Subject 14	29.86	Male	Fetal aortic stenosis with evolving HLHS, single-ventricle physiology
Subject 15	28.00	Male	TOF with pulmonary atresia and multiple aortopulmonary collateral arteries
Subject 16	27.00	Female	Severely unbalanced, right dominant, common AVC, DORV, pulmonary atresia, heterotaxy
Subject 17	26.86	Female	HLHS with intact atrial septum
Subject 18	28.29	Female	Tricuspid and pulmonary atresia
Subject 19	26.71	Female	Coarctation of the aorta with VSD
Subject 20	23.29	Female	Control
Subject 21	25.71	Male	Control
Subject 22	26.14	Female	Control
Subject 23	27.00	Female	Control
Subject 24	29.57	Female	Control
Subject 25	26.43	Female	Control
Subject 26	27.57	Male	Control
Subject 27	23.43	Male	Control
Subject 28	26.29	Female	Control
Subject 29	25.29	Female	Control
Subject 30	26.71	Male	Control
Subject 31	26.86	Female	Control
Subject 32	25.14	Male	Control
Subject 33	26.57	Male	Control
Subject 34	24.57	Male	Control
Subject 35	28.57	Male	Control
Subject 36	27.14	Male	Control

Note: AVC, atrioventricular canal; DORV, double-outlet right ventricle; d-TGA, dextro-transposition of the great arteries; HLHS, hypoplastic left heart syndrome; TOF, tetralogy of Fallot; VSD, ventricular septal defect.

normal range, therefore this finding was deemed a normal variant in both cases.

### Sulcal Pattern Comparison between TD and CHD Fetuses

The  $SI$ ,  $SI_a$ , and  $SI_b$  did not differ between groups for the combined features of the right hemisphere. However, the CHD fetuses had a lower  $SI$  and  $SI_b$  in the left hemisphere compared with the left hemisphere of TD fetuses. Analysis of the individual sulcal basin features for the left hemisphere demonstrated the CHD fetuses to have a lower  $SI$ ,  $SI_a$ , and  $SI_b$  for 3D position. When adjusting for GWs at MRI, these findings persisted, with the exception of  $SI_b$  for 3D position, which only trended toward significance after FDR correction. When individual sulcal basin features were examined for the right hemisphere, only the  $SI_a$  for sulcal depth was significant. However, this association did not persist after FDR correction. Table 2 shows all statistical tests of sulcal pattern similarity between TD and CHD fetuses for different feature sets such as sulcal position, area, and depth and the combination of all features. Sex-specific results demonstrated altered sulcal patterns in the left hemisphere for both male and female fetuses with CHD. However, the primary group differences between TD and CHD fetuses appear to be driven mostly by the female population, whereas males have less significant alterations but effects are also seen in the depth of sulcal basins (Supplementary Table 1).

Regional analyses of the SF and early- and late-emerging sulci were only performed for the left hemisphere combined features and 3D position, as these measures demonstrated group differences in the primary analysis. Regional analysis demonstrated CHD fetuses to have a lower  $SI$  and  $SI_a$  for the combined features of the SF and a lower  $SI_a$  for 3D position in this region.  $SI_b$  could not be tested for the SF because only one sulcal basin was present therefore intersulcal relationships could not be measured for many fetuses. For early- and late-emerging sulci, CHD fetuses had a lower  $SI$ ,  $SI_a$ , and  $SI_b$  for 3D position. Additionally, CHD fetuses had a lower  $SI_b$  for the combined features in late-emerging sulci (Table 3).

Individual surfaces were evaluated to further explore the differences in sulcal basins. A subset of these individual surfaces are displayed in Figure 2. Supplementary Figure 2 demonstrates the individual surfaces, sulcal basins, and similarity indices for all subjects. These images show the CHD fetuses to have differences in the number and location of sulcal basins across multiple regions of the brain. For example, only one sulcal basin in the SF is present at 22, 24, and 26 GWs and only two sulcal basins in the SF at 29 GWs in the individual surfaces of CHD fetuses. In contrast, the TD fetuses have two sulcal basins in the SF at 23 GWs, three at 24 GWs, and four at 25 and 29 GWs. The template brains also have a higher number of sulcal basins in the SF, showing two basins at 23 GWs, three at 24–26 GWs, and six at 29 GWs.

### Comparison of “Standard” Surface-based Measures between TD and CHD Fetuses

The surface-based measures of GI, mean curvature, and cortical surface area did not differ between TD and CHD fetuses for the left or right hemisphere, even after controlling for gestational age at MRI (Table 4).

### Discussion

Our data expand the existing literature on cerebral cortical development in CHD fetuses by defining the spatial, geometric, and topological relationships of sulcation in the second and third trimesters of pregnancy. We have identified CHD fetuses to have global sulcal pattern differences in the left hemisphere compared with TD fetuses. These sulcal pattern differences appear to be driven primarily by differences in the 3D position of sulcal basins. Importantly, altered sulcal patterns existed for the SF and early-emerging sulci, reflecting disturbances as early as the second trimester.

Within the CHD literature, there has been increasing evidence of disturbances in the typical trajectory of cerebral cortical development. Postnatal preoperative MRI data have qualitatively demonstrated simplified gyrification (Licht et al. 2009; Ortinau et al.

**Table 2** Sulcal pattern similarity between TD and CHD groups

	Left hemisphere				Right hemisphere			
	TD	CHD	P-value (t-test)	P-value (regression)	TD	CHD	P-value (t-test)	P-value (regression)
<b>SI</b>								
Combined features	0.822 (0.023)	0.795 (0.030)	0.006*	0.002*	0.818 (0.014)	0.809 (0.026)	0.175	0.415
3D position	0.875 (0.021)	0.856 (0.017)	0.005*	0.008*	0.872 (0.019)	0.866 (0.022)	0.407	0.620
Sulcal basin area	0.918 (0.019)	0.908 (0.045)	0.405	0.083	0.922 (0.017)	0.917 (0.032)	0.576	0.231
Sulcal depth	0.932 (0.019)	0.923 (0.012)	0.093	0.138	0.930 (0.013)	0.926 (0.016)	0.406	0.562
<b>SI<sub>a</sub></b>								
Combined features	0.760 (0.034)	0.741 (0.051)	0.207	0.106	0.771 (0.028)	0.756 (0.047)	0.267	0.241
3D position	0.894 (0.019)	0.876 (0.019)	0.007*	0.002*	0.900 (0.014)	0.895 (0.015)	0.298	0.386
Sulcal basin area	0.807 (0.037)	0.797 (0.059)	0.583	0.358	0.820 (0.035)	0.802 (0.058)	0.264	0.173
Sulcal depth	0.940 (0.016)	0.934 (0.015)	0.200	0.334	0.945 (0.013)	0.933 (0.016)	0.019	0.024
<b>SI<sub>b</sub></b>								
Combined features	0.832 (0.023)	0.807 (0.023)	0.003*	0.003*	0.827 (0.015)	0.819 (0.022)	0.236	0.339
3D position	0.872 (0.022)	0.854 (0.018)	0.009*	0.015	0.867 (0.019)	0.861 (0.022)	0.429	0.608
Sulcal basin area	0.937 (0.015)	0.929 (0.029)	0.352	0.145	0.940 (0.013)	0.938 (0.019)	0.712	0.546
Sulcal depth	0.930 (0.020)	0.920 (0.013)	0.066	0.083	0.927 (0.013)	0.924 (0.017)	0.497	0.597

Note: Data: mean (standard deviation).  $SI$ : similarity of the whole sulcal pattern,  $SI_a$ : similarity between corresponding sulcal basins,  $SI_b$ : similarity of intersulcal relationship. The P-value for the regression model includes gestational age at MRI as a covariate. An FDR correction was applied for P-values. \*Corrected  $P < 0.05$  with FDR correction.

**Table 3** Subanalyses for the left hemisphere SF and the early- and late-Emerging sulci

		TD	CHD	P-value (t-test)	P-value (regression)
<b>SF</b>					
SI	Combined features	0.789 (0.046)	0.683 (0.169)	0.015*	0.001*
	3D position	0.886 (0.036)	0.861 (0.047)	0.080	0.057
SI <sub>a</sub>	Combined features	0.748 (0.056)	0.656 (0.156)	0.025*	0.003*
	3D position	0.895 (0.028)	0.867 (0.049)	0.048*	0.019*
<b>Early-emerging sulci</b>					
SI	Combined features	0.813 (0.031)	0.799 (0.030)	0.181	0.182
	3D position	0.881 (0.028)	0.861 (0.017)	0.013*	0.018*
SI <sub>a</sub>	Combined features	0.754 (0.054)	0.751 (0.049)	0.868	0.876
	3D position	0.897 (0.024)	0.878 (0.019)	0.011*	0.006*
SI <sub>b</sub>	Combined features	0.831 (0.029)	0.815 (0.026)	0.077	0.103
	3D position	0.876 (0.031)	0.857 (0.018)	0.027*	0.033*
<b>Late-emerging sulci</b>					
SI	Combined features	0.832 (0.026)	0.816 (0.053)	0.323	0.420
	3D position	0.890 (0.031)	0.860 (0.033)	0.017*	0.039*
SI <sub>a</sub>	Combined features	0.803 (0.042)	0.796 (0.062)	0.726	0.943
	3D position	0.901 (0.023)	0.880 (0.027)	0.034*	0.042*
SI <sub>b</sub>	Combined features	0.853 (0.036)	0.814 (0.050)	0.029*	0.032*
	3D position	0.884 (0.048)	0.844 (0.040)	0.026*	0.030*

Note: Data: mean (standard deviation). SI: similarity of the whole sulcal pattern, SI<sub>a</sub>: similarity between corresponding sulcal basins, SI<sub>b</sub>: similarity of intersulcal relationships. The SI<sub>b</sub> was not examined for the SF since several early gestation fetuses have only one sulcal basin in the SF. This is represented by a dash. Because of the early gestational ages of some fetuses, only 14 TD and 16 CHD fetuses were able to be included in the analysis for late-emerging sulci for SI and SI<sub>a</sub>, and only 14 TD and 13 TD for SI<sub>b</sub>. The P-value for the regression model includes gestational age at MRI as a covariate. \*P-values < 0.05.

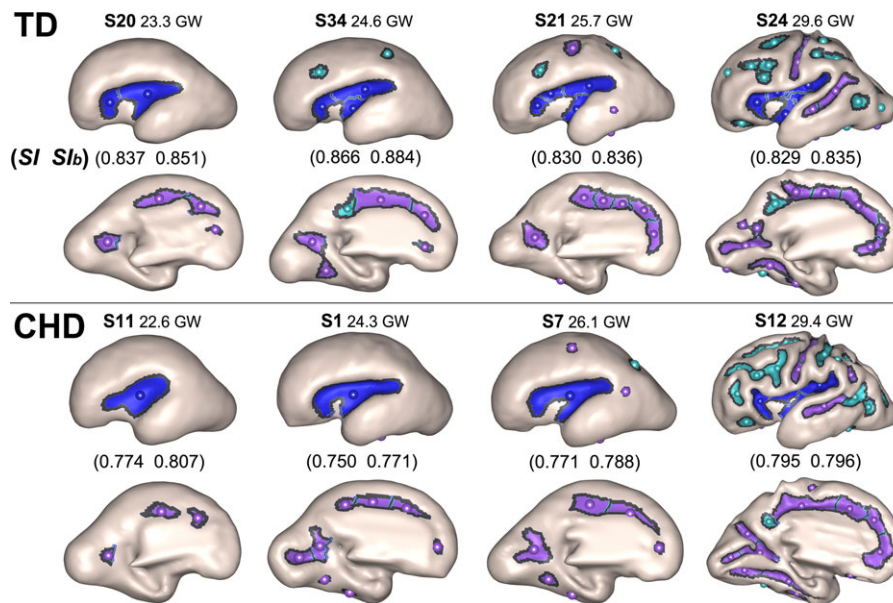


**Figure 2.** Individual fetal surfaces for TD fetuses are on the top and CHD fetuses are at the bottom. Each circle represents a sulcal basin in each region for the SF (blue), early-emerging sulci (purple), and late-emerging sulci (aqua). The figure demonstrates the differences in the number and spatial distribution of sulcal basins for each individual at varying gestational ages, particularly for the SF, although other regions are also affected.

2012). Quantitative cortical analyses have further characterized these qualitative abnormalities by demonstrating decreased GI, decreased cortical surface area, and altered sulcal depth in CHD infants imaged preoperatively (Ortinau et al. 2013). These data support the possibility of prenatal disruption of cortical development. Likewise, preliminary fetal MRI data have begun to confirm this hypothesis. Specifically, CHD fetuses imaged during the late third trimester, at 36–38 GWs, displayed decreased sulcal depth in the left and right parieto-occipital, cingulate, and calcarine

fissures and in the left insular lobe (Masoller et al. 2016). In addition, Clouchoux and colleagues demonstrated reductions in GI and cortical surface area in fetuses with hypoplastic left heart syndrome, one of the most severe forms of CHD. While the alterations in GI and cortical surface area were not present until after 30 GWs, sulcation and cortical depth abnormalities existed across multiple regions of the brain starting at 25–27 GWs in that cohort. Those data showed a 3-week delayed appearance of the SFS, anterior ascending ramus, and the CiS (Clouchoux et al.



**Table 4** Surface-based measures between TD and CHD groups

	TD	CHD	P (t-test)	P (regression)
Left hemisphere				
GI	1.127 (0.043)	1.152 (0.056)	0.158	0.178
Mean curvature	0.092 (0.010)	0.098 (0.019)	0.209	0.510
Surface area (mm <sup>2</sup> )	7596.6 (1373.7)	8265.6 (2481.3)	0.264	0.645
Right hemisphere				
GI	1.126 (0.040)	1.149 (0.055)	0.193	0.215
Mean curvature	0.090 (0.010)	0.096 (0.019)	0.244	0.576
Surface area (mm <sup>2</sup> )	7604.2 (1340.6)	8301.4 (2465.1)	0.244	0.543

Note: data: mean (standard deviation). The P-value for the regression model includes gestational age at MRI as a covariate.

2013). Similar to this work, our data did not identify differences in GI or cortical surface area before 30 GWs but did demonstrate differences in the sulcal patterns. Importantly, our findings extend knowledge of sulcal depth patterns by identifying differences in the 3D position of sulcal basins for both corresponding sulci and intersulcal relationships. These patterns of alterations are present in our cohort at earlier gestational ages (as early as 22 GWs on individual surfaces) than has previously been reported. This suggests that methods for evaluating the relationships of sulcation and global sulcal pattern may be more sensitive than traditional sulcal depth (and other surface-based) methods for detecting earlier and more subtle alterations in cortical development.

The sulcal pattern alterations present in our cohort are primarily in the left hemisphere. Hemispheric asymmetries are a common feature of typical brain development and are associated with differential gene expression, even as early as 12–14 GWs (Sun et al. 2005; Sun and Hevner 2014). The temporal lobe and SF are key areas of asymmetry that have been characterized on fetal MRI, with sulcation in the right STS emerging approximately 1–2 weeks prior to the left (Kasprian et al. 2011; Habas et al. 2012). Specific to the CHD population, we have previously identified sulcal depth differences primarily in the left hemisphere of infants with complex CHD prior to cardiac surgery (Ortinou et al. 2013). In the prenatal setting, hypoplastic left heart syndrome fetuses appear to be lacking the major asymmetries seen in control fetuses, particularly in the temporal lobe (Clouchoux et al. 2013). Our results demonstrate CHD fetuses to have less similarity to template brains specifically for the 3D position of sulcal basins in the left SF. The perisylvian region has been identified as a particularly vulnerable brain region in patients with CHD based on both postmortem and imaging studies reporting a high prevalence of an open operculum in infants with CHD (Glauser et al. 1990; Mahle et al. 2002; Licht et al. 2009). Fetal ultrasonography has also identified reduced brain fissure depth including reductions in the SF (Peng et al. 2016). Fetal MRI has reported a lack of hemispheric asymmetry in the temporal lobe and in the posterior region of the SF (Clouchoux et al. 2013), as well as decreased sulcal depth in the left insular lobe (Masoller et al. 2016). Our analyses of individual brains showing fewer sulcal basins and altered sulcal pattern in the SF of the left hemisphere in CHD fetuses compared with TD fetuses suggest a particular vulnerability of this region that may reflect an impairment in the typical development of hemispheric asymmetries.

With regard to the timing of altered sulcal patterns, we separately examined early and late-emerging sulci. Primary sulcation begins in the early second trimester and continues to progress into the third trimester, along with the formation of

secondary sulci. Tertiary sulci begin to form in the third trimester and are still developing even after birth. The primary sulcal pattern is likely to be prenatally determined with little individual variability before 30 GWs (Chi et al. 1977; Garel et al. 2001; Rakic 2004; Kostovic and Vasung 2009; Stiles and Jernigan 2010). Despite this, our data demonstrate clear differences in sulcal patterns in CHD fetuses at <30 GWs. In addition, differences were present even for early-emerging sulci, which typically develop prior to 24 GWs. Prior imaging work has shown an average lag of 2 weeks between the time when sulci are detected on postmortem tissue samples and when they are visible on fetal MRI (Habas et al. 2012). Thus, our findings of differences even in early-emerging sulci may suggest that sulcation in CHD fetuses can be affected as early as the beginning of the second trimester, when the first-emerging sulci under tight genetic control are developing.

Individual surfaces (Supplementary Fig. 2) not only demonstrated altered sulcal patterns early in gestation but also highlighted the variability and evolution of sulcal pattern over gestation. The earliest gestational ages clearly demonstrate CHD fetuses to have fewer sulcal pits with altered position and patterning compared with TD fetuses. As gestation progresses, this becomes less visibly apparent, particularly near 27 GWs. By 28–30 GWs, some CHD fetuses visibly demonstrate greater complexity of cortical folding but with patterns that were often less similar to template brains than TD fetuses. Our prior work in CHD infants demonstrated altered cortical development with some regions displaying decreased sulcal depth, while others showed increased sulcal depth, reflective of a broader more open sulcus (Ortinou et al. 2013). Additionally, increased sulcation has been reported in growth-restricted infants who also displayed decreased cortical thickness, suggesting that cortical thickness might affect the biomechanical mechanisms of cortical folding discussed below (Dubois et al. 2008). Although cortical thickness was not measured in our study, our findings, in the context of this prior work, emphasize the complexity of cortical development as a likely multifactorial process in non-TD fetuses.

While our data have extended existing knowledge of the timing and pattern of cortical alterations, the pathophysiology driving these alterations in sulcal architecture remains unclear. Several hypotheses have been proposed as potential mechanisms of cortical folding and sulcal pattern development. These include mechanical folding by differential growth of superficial and deep layers of the brain (Richman et al. 1975; Toro and Burnod 2005; Budday et al. 2014; Tallinen et al. 2016), axonal tension in the white matter between nearby cortical areas (Van Essen 1997; Hilgetag and Barbas 2006), and differential cortical expansion related to cytoarchitecture (Welker 1990; Ronan and Fletcher 2015). As the primary pattern of cortical



sulcal folds appears to be prenatally determined and highly stereotyped (Kostovic and Vasung 2009; White et al. 2010), it is thought that this pattern is influenced by different expression patterns of various genes according to the cortical regions and layers (Leary et al. 2007; de Juan Romero and Borrell 2017). Additionally, the primary sulcal pattern has been associated with organization of cortical functional areas and their white matter connections (Van Essen 1997; Klyachko and Stevens 2003; Rakic 2004; O'Leary et al. 2007; Fischl et al. 2008; Sun and Hevner 2014; Ronan and Fletcher 2015; Fernandez et al. 2016).

Recent data in CHD patients have linked the presence of genetic variants with adverse neurodevelopmental outcomes (Homsy et al., 2015). However, the connections between genomics, altered cortical development, and adverse neurodevelopment in CHD have yet to be made. Adult literature has suggested higher heritability of brain structures that appear earlier in development (Brun et al. 2008), and differential gene expression appears to regulate the typical development of hemispheric asymmetries (Sun et al. 2005; Sun and Hevner 2014). In addition, the geometric and topological pattern analysis of early cortical folds has proven effective for characterizing genetically influenced early cortical development in several of our previous studies (Im et al. 2010, 2016, 2017; Im, Choi, et al. 2011; Im, Pienaar, Lee et al. 2011, 2013). Of particular relevance is our data showing altered intersulcal relationships in fetuses with agenesis of the corpus callosum, a diagnosis commonly associated with genetic causes (Tarui et al. 2018). Thus, our findings of abnormalities in the intersulcal relationships of 3D position in the early-emerging sulci, in combination with hemispheric asymmetries in sulcal pattern effects, could suggest that genetic variants and/or alterations in gene expression are important determinants of the differences in cortical region- and layer-specific areal expansion, causing the sulcal pattern differences identified.

An alternative mechanism for altered cortical development relates to the cardiac defect itself affecting cerebral oxygenation, perfusion, and/or nutrient delivery. This hypothesis can be compared with the preterm data where infants display white matter injury, from hypoxic-ischemic cerebral insults, followed by cortical volumetric deficits and abnormalities in cortical folding (Inder et al. 1999; Shimony et al. 2016). Similar to preterm infants, infants with CHD display high rates of white matter injury and cortical gray matter derangements (Volpe 2014). Therefore, cerebral hypoxia, hypoperfusion, or impaired nutrient delivery may result in injury or trophic effects in the CHD fetus. Prior work has demonstrated impaired cerebral hemodynamics and brain biometry as early as 22 GWs in fetuses with CHD (Masoller et al. 2016). Recent fetal MR data have also shown reduced cerebral oxygenation and impaired oxygen consumption in fetuses with CHD (Sun et al. 2015; Lauridsen et al. 2017). A porcine chronic hypoxia model has demonstrated impaired neurogenesis in the subventricular zone, accompanied by decreased interneurons in the prefrontal cortex with corresponding decreased cortical volume and gyrification of this region. Similar findings were apparent in human pathology specimens (Morton et al. 2017). This work supports the hypothesis that white matter injury via cerebral hypoxia could affect axonal development and impair biomechanical pathways of cortical development related to axonal tension. As recently proposed by Rudolph, it is also possible that disrupted hemodynamics influence brain development via impaired glucose delivery secondary to reduced cerebral perfusion (in the fetus with HLHS) or to changes in distribution of glucose-rich blood from the umbilical vein (in the fetus with TGA) (Rudolph

2016). Despite data supporting an important role of physiologic disruption of cortical development, cortical alterations have been shown to precede volumetric deficits of the white matter in hypoplastic left heart syndrome, a finding suggestive of genetic origins (Clouchoux et al. 2013). Thus, a potentially more likely mechanistic possibility is that the differences we identified in sulcal patterns reflect altered gene expression modulated by abnormal cardiac physiology.

Our study has several limitations. First, in this exploratory analysis, our sample size is small. Although the results are promising in that we were able to detect statistically significant differences in sulcal pattern development, a larger cohort is needed to confirm these findings and provide more detailed analyses. Second, our cohort includes a heterogeneous sample of CHD fetuses. The heterogeneity of diagnoses may obscure important differences between cardiac subgroups. With a larger sample size, we will be able to compare between cardiac diagnoses/physiologies to determine the highest risk populations of CHD fetuses and to test the hypothesis that altered cardiac hemodynamics are associated with altered cortical development. While our results suggest an important role for genetics in cortical patterning in CHD, the lack of genetic data prohibit us from directly evaluating genetic variants as a potential mechanism for the alterations identified. Because we focused on whether our measures were sensitive to early differences in cortical development, our cohort only includes analyses of fetuses up to 30 GWs. Longitudinal assessments of cortical development in CHD fetuses are necessary to determine whether these changes persist and/or evolve over the course of the pregnancy, which may also provide mechanistic insights. Finally, our fetal MRI analysis incorporates smoothing and thresholding methods to limit noise in the data associated with motion, poor signal to noise ratio, and other factors. While this likely decreases the chance of a type I error, it may also obscure more subtle structural differences. Despite these limitations, our study has identified cortical disturbances at an earlier gestational age than previously reported, and, in combination with the pattern of abnormalities and the presence of hemispheric asymmetries, suggests genetic/epigenetic factors may be mechanistically important.

## Supplementary Material

Supplementary material is available at *Cerebral Cortex* online.

## Funding

The Mend A Heart Foundation (to C.M.O.); the Children's Discovery Institute of Washington University and St. Louis Children's Hospital (to C.M.O.); a Scholar Award from the Pediatric Heart Network (PHN) supported by the National Heart, Lung, and Blood Institute of the National Institutes of Health (grant U10HL068270 to C.K.R.); a Neurological Sciences Academic Developmental Award from the National Institute of Neurological Disorders and Stroke (to C.K.R.); the National Institute of Neurological Disorders and Stroke (grant K23NS101120 to C.K.R.); the Eunice Kennedy Shriver National Institute of Child Health & Human Development of the National Institutes of Health (grant R21HD083956 to K.I. and grant U01HD087211 to P.E.G.); the National Institute of Biomedical Imaging and Bioengineering of the National Institutes of Health (R01EB013248 to S.K.W., R01EB018988 to A.G., R01EB017337 to P.E.G.); a 2017 NARSAD Distinguished Investigator Grant from the Brain and Behavior Research Foundation (to S.K.W.); the McKnight

Foundation Technological Innovations in Neuroscience Award (to A.G.); Career Development Awards from the Office of Faculty Development at Boston Children's Hospital (to A.G. and K.I.); and an American Academy of Neurology Clinical Research Training Fellowship (to C.K.R.). The content of this work is solely the responsibility of the authors and does not necessarily represent the official views of the National Institutes of Health.

## Notes

*Conflict of Interest:* None declared.

## References

- Alfif A, Bouvier R, Buenerd A, Trouillas J, Mertens P. 2007. Development of the human fetal insular cortex: study of the gyration from 13 to 28 gestational weeks. *Brain Struct Funct.* 212:335–346.
- Algra SO, Haas F, Poskitt KJ, Groenendaal F, Schouten AN, Jansen NJ, Azakie A, Gandhi S, Campbell A, Miller SP, et al. 2014. Minimizing the risk of preoperative brain injury in neonates with aortic arch obstruction. *J Pediatr.* 165:1116–1122 e1113.
- Awate SP, Yushkevich P, Song Z, Licht D, Gee JC. 2009. Multivariate high-dimensional cortical folding analysis, combining complexity and shape, in neonates with congenital heart disease. *Inf Process Med Imaging.* 21:552–563.
- Beca J, Gunn JK, Coleman L, Hope A, Reed PW, Hunt RW, Finucane K, Brizard C, Dance B, Shekerdemian LS. 2013. New white matter brain injury after infant heart surgery is associated with diagnostic group and the use of circulatory arrest. *Circulation.* 127:971–979.
- Bellinger DC, Wypij D, Rivkin MJ, DeMaso DR, Robertson RL Jr., Dunbar-Masterson C, Rappaport LA, Wernovsky G, Jonas RA, Newburger JW. 2011. Adolescents with d-transposition of the great arteries corrected with the arterial switch procedure: neuropsychological assessment and structural brain imaging. *Circulation.* 124:1361–1369.
- Benjamini Y, Hochberg Y. 1995. Controlling the false discovery rate—a practical and powerful approach to multiple testing. *J Roy Stat Soc B Met.* 57:289–300.
- Brossard-Racine M, du Plessis A, Vezina G, Robertson R, Donofrio M, Tworetzky W, Limperopoulos C. 2016. Brain injury in neonates with complex congenital heart disease: what is the predictive value of MRI in the fetal period? *AJNR Am J Neuroradiol.* 37:1338–1346.
- Brun C, Lepore N, Pennec X, Chou YY, Lee AD, Barysheva M, de Zubicaray G, Meredith M, McMahon K, Wright MJ, et al. 2008. A tensor-based morphometry study of genetic influences on brain structure using a new fluid registration method. *Med Image Comput Comput Assist Interv.* 11:914–921.
- Budday S, Steinmann P, Kuhl E. 2014. The role of mechanics during brain development. *J Mech Phys Solids.* 72:75–92.
- Chi JG, Dooling EC, Gilles FH. 1977. Gyral development of the human brain. *Ann Neurol.* 1:86–93.
- Chung MK, Robbins SM, Dalton KM, Davidson RJ, Alexander AL, Evans AC. 2005. Cortical thickness analysis in autism with heat kernel smoothing. *Neuroimage.* 25:1256–1265.
- Clouchoux C, du Plessis AJ, Bouyssi-Kobar M, Tworetzky W, McElhinney DB, Brown DW, Gholipour A, Kudelski D, Warfield SK, McCarter RJ, et al. 2013. Delayed cortical development in fetuses with complex congenital heart disease. *Cereb Cortex.* 23:2932–2943.
- Cox RW. 2012. AFNI: what a long strange trip it's been. *Neuroimage.* 62:743–747.
- de Juan Romero C, Borrell V. 2017. Genetic maps and patterns of cerebral cortex folding. *Curr Opin Cell Biol.* 49:31–37.
- Derrfuss J, Brass M, von Cramon DY, Lohmann G, Amunts K. 2009. Neural activations at the junction of the inferior frontal sulcus and the inferior precentral sulcus: interindividual variability, reliability, and association with sulcal morphology. *Hum Brain Mapp.* 30:299–311.
- Dubois J, Benders M, Borradori-Tolsa C, Cachia A, Lazeyras F, Ha-Vinh Leuchter R, Sizonenko SV, Warfield SK, Mangin JF, Huppi PS. 2008. Primary cortical folding in the human newborn: an early marker of later functional development. *Brain.* 131:2028–2041.
- Fernandez V, Llinares-Benadero C, Borrell V. 2016. Cerebral cortex expansion and folding: what have we learned? *EMBO J.* 35:1021–1044.
- Fischl B. 2012. FreeSurfer. *Neuroimage.* 62:774–781.
- Fischl B, Rajendran N, Busa E, Augustinack J, Hinds O, Yeo BT, Mohlberg H, Amunts K, Zilles K. 2008. Cortical folding patterns and predicting cytoarchitecture. *Cereb Cortex.* 18:1973–1980.
- Fogliarini C, Chaumoitre K, Chapon F, Fernandez C, Levrier O, Figarella-Branger D, Girard N. 2005. Assessment of cortical maturation with prenatal MRI: part II: abnormalities of cortical maturation. *Eur Radiol.* 15:1781–1789.
- Garel C, Chantrel E, Brisse H, Elmaleh M, Luton D, Oury JF, Sebag G, Hassan M. 2001. Fetal cerebral cortex: normal gestational landmarks identified using prenatal MR imaging. *AJNR Am J Neuroradiol.* 22:184–189.
- Genovese CR, Lazar NA, Nichols T. 2002. Thresholding of statistical maps in functional neuroimaging using the false discovery rate. *Neuroimage.* 15:870–878.
- Gholipour A, Estroff JA, Warfield SK. 2010. Robust super-resolution volume reconstruction from slice acquisitions: application to fetal brain MRI. *IEEE Trans Med Imaging.* 29:1739–1758.
- Gholipour A, Rollins CK, Velasco-Annis C, Ouassal A, Akhondiasl A, Afacan O, Ortinau CM, Clancy S, Limperopoulos C, Yang E, et al. 2017. A normative spatiotemporal MRI atlas of the fetal brain for automatic segmentation and analysis of early brain growth. *Sci Rep.* 7:476.
- Glauser TA, Rorke LB, Weinberg PM, Clancy RR. 1990. Congenital brain anomalies associated with the hypoplastic left heart syndrome. *Pediatrics.* 85:984–990.
- Goldberg CS, Lu M, Sleeper LA, Mahle WT, Gaynor JW, Williams IA, Mussatto KA, Ohye RG, Graham EM, Frank DU, et al. Pediatric Heart Network I. 2014. Factors associated with neurodevelopment for children with single ventricle lesions. *J Pediatr.* 165:490–496 e498.
- Guibaud L, Salleret L, Larroche JC, Buenerd A, Alias F, Gaucherand P, Des Portes V, Pracros JP. 2008. Abnormal Sylvian fissure on prenatal cerebral imaging: significance and correlation with neuropathological and postnatal data. *Ultrasound Obstet Gynecol.* 32:50–60.
- Habas PA, Scott JA, Roosta A, Rajagopalan V, Kim K, Rousseau F, Barkovich AJ, Glenn OA, Studholme C. 2012. Early folding patterns and asymmetries of the normal human brain detected from in utero MRI. *Cereb Cortex.* 22:13–25.
- Hilgetag CC, Barbas H. 2006. Role of mechanical factors in the morphology of the primate cerebral cortex. *PLoS Comput Biol.* 2:e22.
- Hoffman JI, Kaplan S. 2002. The incidence of congenital heart disease. *J Am Coll Cardiol.* 39:1890–1900.

- Homsy J, Zaidi S, Shen Y, Ware JS, Samocha KE, Karczewski KJ, DePalma SR, McKean D, Wakimoto H, Gorham J, et al. 2015. De novo mutations in congenital heart disease with neurodevelopmental and other congenital anomalies. *Science*. 350:1262–1266.
- Im K, Choi YY, Yang JJ, Lee KH, Kim SI, Grant PE, Lee JM. 2011. The relationship between the presence of sulcal pits and intelligence in human brains. *Neuroimage*. 55:1490–1496.
- Im K, Guimaraes A, Kim Y, Cottrill E, Gagoski B, Rollins C, Ortinau C, Yang E, Grant PE. 2017. Quantitative folding pattern analysis of early primary sulci in human fetuses with brain abnormalities. *AJNR Am J Neuroradiol*. 38:1449–1455.
- Im K, Jo HJ, Mangin JF, Evans AC, Kim SI, Lee JM. 2010. Spatial distribution of deep sulcal landmarks and hemispherical asymmetry on the cortical surface. *Cereb Cortex*. 20:602–611.
- Im K, Lee JM, Jeon S, Kim JH, Seo SW, Na DL, Grant PE. 2013. Reliable identification of deep sulcal pits: the effects of scan session, scanner, and surface extraction tool. *PLoS One*. 8:e53678.
- Im K, Pienaar R, Lee JM, Seong JK, Choi YY, Lee KH, Grant PE. 2011. Quantitative comparison and analysis of sulcal patterns using sulcal graph matching: a twin study. *Neuroimage*. 57:1077–1086.
- Im K, Pienaar R, Paldino MJ, Gaab N, Galaburda AM, Grant PE. 2013. Quantification and discrimination of abnormal sulcal patterns in polymicrogyria. *Cereb Cortex*. 23:3007–3015.
- Im K, Raschle NM, Smith SA, Ellen Grant P, Gaab N. 2016. Atypical sulcal pattern in children with developmental dyslexia and at-risk kindergarteners. *Cereb Cortex*. 26:1138–1148.
- Inder TE, Huppi PS, Warfield S, Kikinis R, Zientara GP, Barnes PD, Jolesz F, Volpe JJ. 1999. Periventricular white matter injury in the premature infant is followed by reduced cerebral cortical gray matter volume at term. *Ann Neurol*. 46:755–760.
- Kasprian G, Langs G, Brugger PC, Bittner M, Weber M, Arantes M, Prayer D. 2011. The prenatal origin of hemispheric asymmetry: an in utero neuroimaging study. *Cereb Cortex*. 21:1076–1083.
- Klyachko VA, Stevens CF. 2003. Connectivity optimization and the positioning of cortical areas. *Proc Natl Acad Sci USA*. 100:7937–7941.
- Kostovic I, Vasung L. 2009. Insights from in vitro fetal magnetic resonance imaging of cerebral development. *Semin Perinatol*. 33:220–233.
- Kuklisova-Murgasova M, Quaghebeur G, Rutherford MA, Hajnal JV, Schnabel JA. 2012. Reconstruction of fetal brain MRI with intensity matching and complete outlier removal. *Med Image Anal*. 16:1550–1564.
- Lauridsen MH, Uldbjerg N, Henriksen TB, Petersen OB, Stausbol-Gron B, Matthiesen NB, Peters DA, Ringgaard S, Hjortdal VE. 2017. Cerebral oxygenation measurements by magnetic resonance imaging in fetuses with and without heart defects. *Circ Cardiovasc Imaging*. 10:e006459.
- Leordeanu M, Hebert M. 2005. A spectral technique for correspondence problems using pairwise constraints. ICCV '05: Proceedings of the Tenth IEEE International Conference on Computer Vision IEEE Computer Society, Washington, DC, USA:1482–1489.
- Lerman-Sagie T, Malinger G. 2008. Focus on the fetal Sylvian fissure. *Ultrasound Obstet Gynecol*. 32:3–4.
- Licht DJ, Shera DM, Clancy RR, Wernovsky G, Montenegro LM, Nicolson SC, Zimmerman RA, Spray TL, Gaynor JW, Vossough A. 2009. Brain maturation is delayed in infants with complex congenital heart defects. *J Thorac Cardiovasc Surg*. 137:529–536. discussion 536–527.
- Limperopoulos C, Tworetzky W, McElhinney DB, Newburger JW, Brown DW, Robertson RL Jr., Guizard N, McGrath E, Geva J, Annese D, et al. 2010. Brain volume and metabolism in fetuses with congenital heart disease: evaluation with quantitative magnetic resonance imaging and spectroscopy. *Circulation*. 121:26–33.
- Mahle WT, Tavani F, Zimmerman RA, Nicolson SC, Galli KK, Gaynor JW, Clancy RR, Montenegro LM, Spray TL, Chiavacci RM, et al. 2002. An MRI study of neurological injury before and after congenital heart surgery. *Circulation*. 106:I109–I114.
- Majnemer A, Limperopoulos C, Shevell M, Rohlicek C, Rosenblatt B, Tchervenkov C. 2008. Developmental and functional outcomes at school entry in children with congenital heart defects. *J Pediatr*. 153:55–60.
- Masoller N, Sanz-Cortes M, Crispi F, Gomez O, Bannasar M, Egana-Ugrinovic G, Bargallo N, Martinez JM, Gratacos E. 2016. Severity of fetal brain abnormalities in congenital heart disease in relation to the main expected pattern of in utero brain blood supply. *Fetal Diagn Ther*. 39:269–278.
- Miatton M, De Wolf D, Francois K, Thiery E, Vingerhoets G. 2007. Neuropsychological performance in school-aged children with surgically corrected congenital heart disease. *J Pediatr*. 151:73–78, 78 e71.
- Miller SP, McQuillen PS, Hamrick S, Xu D, Glidden DV, Charlton N, Karl T, Azakie A, Ferriero DM, Barkovich AJ, et al. 2007. Abnormal brain development in newborns with congenital heart disease. *N Engl J Med*. 357:1928–1938.
- Morton PD, Korotcova L, Lewis BK, Bhuvanendran S, Ramachandra SD, Zurakowski D, Zhang J, Mori S, Frank JA, Jonas RA, et al. 2017. Abnormal neurogenesis and cortical growth in congenital heart disease. *Sci Transl Med*. 9:eaah7029.
- Ortinau C, Alexopoulos D, Dierker D, Van Essen D, Beca J, Inder T. 2013. Cortical folding is altered before surgery in infants with congenital heart disease. *J Pediatrics*. 163:1507–1510.
- Ortinau C, Beca J, Lambeth J, Ferdman B, Alexopoulos D, Shimony JS, Wallendorf M, Neil J, Inder T. 2012. Regional alterations in cerebral growth exist preoperatively in infants with congenital heart disease. *J Thorac Cardiovasc Surg*. 143:1264–1270.
- O'Leary DD, Chou SJ, Sahara S. 2007. Area patterning of the mammalian cortex. *Neuron*. 56:252–269.
- Peng Q, Zhou Q, Zang M, Zhou J, Xu R, Wang T, Zeng S. 2016. Reduced fetal brain fissures depth in fetuses with congenital heart diseases. *Prenat Diagn*. 36:1047–1053.
- Rakic P. 2004. Neuroscience. Genetic control of cortical convolutions. *Science*. 303:1983–1984.
- Richman DP, Stewart RM, Hutchinson JW, Caviness VS Jr. 1975. Mechanical model of brain convolutional development. *Science*. 189:18–21.
- Ronan L, Fletcher PC. 2015. From genes to folds: a review of cortical gyrification theory. *Brain Struct Funct*. 220:2475–2483.
- Rudolph AM. 2016. Impaired cerebral development in fetuses with congenital cardiovascular malformations: is it the result of inadequate glucose supply? *Pediatr Res*. 80:172–177.
- Sarnat HB, Flores-Sarnat L. 2016. Telencephalic flexure and malformations of the lateral cerebral (Sylvian) fissure. *Pediatr Neurol*. 63:23–38.
- Schaer M, Cuadra MB, Tamarit L, Lazeyras F, Eliez S, Thiran JP. 2008. A surface-based approach to quantify local cortical gyrification. *IEEE Trans Med Imaging*. 27:161–170.

- Serag A, Aljabar P, Ball G, Counsell SJ, Boardman JP, Rutherford MA, Edwards AD, Hajnal JV, Rueckert D. 2012. Construction of a consistent high-definition spatio-temporal atlas of the developing brain using adaptive kernel regression. *Neuroimage*. 59:2255–2265.
- Shimony JS, Smyser CD, Wideman G, Alexopoulos D, Hill J, Harwell J, Dierker D, Van Essen DC, Inder TE, Neil JJ. 2016. Comparison of cortical folding measures for evaluation of developing human brain. *Neuroimage*. 125:780–790.
- Stiles J, Jernigan TL. 2010. The basics of brain development. *Neuropsychol Rev*. 20:327–348.
- Sun T, Hevner RF. 2014. Growth and folding of the mammalian cerebral cortex: from molecules to malformations. *Nat Rev Neurosci*. 15:217–232.
- Sun L, Macgowan CK, Sled JG, Yoo SJ, Manhiot C, Porayette P, Grosse-Wortmann L, Jaeggi E, McCrindle BW, Kingdom J, et al. 2015. Reduced fetal cerebral oxygen consumption is associated with smaller brain size in fetuses with congenital heart disease. *Circulation*. 131:1313–1323.
- Sun T, Patoine C, Abu-Khalil A, Visvader J, Sum E, Cherry TJ, Orkin SH, Geschwind DH, Walsh CA. 2005. Early asymmetry of gene transcription in embryonic human left and right cerebral cortex. *Science*. 308:1794–1798.
- Tallinen T, Chung JY, Rousseau F, Girard N, Lefevre J, Mahadevan L. 2016. On the growth and form of cortical convolutions. *Nat Phys*. 12:588–593.
- Tarui T, Madan N, Farhat N, Kitano R, Ceren Tanritanir A, Graham G, Gagoski B, Craig A, Rollins CK, Ortinau C, et al. 2018. Disorganized patterns of sulcal position in fetal brains with agenesis of corpus callosum. *Cereb Cortex*. 28:3192–3203.
- Toro R, Burnod Y. 2005. A morphogenetic model for the development of cortical convolutions. *Cereb Cortex*. 15:1900–1913.
- Van Essen DC. 1997. A tension-based theory of morphogenesis and compact wiring in the central nervous system. *Nature*. 385:313–318.
- Volpe JJ. 2014. Encephalopathy of congenital heart disease—destructive and developmental effects intertwined. *J Pediatr*. 164:962–965.
- Welker W. 1990. Why does cerebral cortex fissure and fold? A review of determinants of gyri and sulci. In: Jones EG, Pertes A, editors. *Cerebral Cortex*. Vol 8B. New York (NY): Plenum. p. 3–136.
- Wernovsky G. 2006. Current insights regarding neurological and developmental abnormalities in children and young adults with complex congenital cardiac disease. *Cardiol Young*. 16(Suppl 1):92–104.
- White T, Su S, Schmidt M, Kao CY, Sapiro G. 2010. The development of gyrification in childhood and adolescence. *Brain Cogn*. 72:36–45.
- Zilles K, Armstrong E, Schleicher A, Kretschmann HJ. 1988. The human pattern of gyrification in the cerebral cortex. *Anat Embryol (Berl)*. 179:173–179.